REFERENCES

1. Okazumi S, Isono K, Enomoto K, et al. Evaluation of liver tumors using fluorine-18-fluorodeoxyglucose PET: characterization of tumor and assessment of effect of treatment. *J Nucl Med* 1992;33:333–339.
2. Okada J, Yoshikawa K, Itami M, et al. Positron emission tomography using fluorine-18-fluorodeoxyglucose in malignant lymphoma: a comparison with proliferate activity. *J Nucl Med* 1992;33:325–329.
3. Messa C, Choi Y, Hoh CK, et al. Quantification of glucose utilization in liver metastases: parametric imaging of FDG uptake with PET. *J Comput Assist Tomogr* 1992;16:684–689.
4. Wahl RL, Cody RL, Hutchins GD, and Mudgett EE. Primary and metastatic breast carcinoma: initial clinical evaluation with PET with the radiolabeled glucose analogue 2-[^{18}F]-fluoro-2-deoxy-D-glucose. *Radiology* 1991;179:765–770.
5. Hawkins RA, Hoh CK, Dahlbom M, et al. PET Cancer Evaluations with FDG [Editorial]. *J Nucl Med* 1991;32:1555–1558.
6. Bares R, Altehoefer C, Cremerius U, et al. FDG-PET for metabolic classification of residual lymphoma masses after chemotherapy [Abstract]. *J Nucl Med* 1994;35:131P.
7. Phelps ME, Huang SC, Hoffman EJ, Selin CJ, Sokoloff L, Kuhl DE. Tomographic measurement of local cerebral glucose metabolic rate in humans with [^{18}]-fluoro-2-deoxy-D-glucose: validation of method. *Ann Neurol* 1979;6:371–388.
8. Huang SC, Phelps ME, Hoffman EJ, Sideris K, Selin CJ, Kuhl DE. Noninvasive determination of local cerebral metabolic rate of glucose in man. *Am J Physiol* 1980;238:E69–E82.
9. Patlak CS, Blasberg RG, Fenstenmacher JD. Graphical evaluation of blood-to-brain transfer constants from multiple-time uptake data. *J Cereb Blood Flow Metab* 1983;3:1–7.
10. Hawkins RA, Choi Y, Huang SC, Messa C, Hoh CK, Phelps ME. Quantitating tumor glucose metabolism with FDG and PET [Editorial]. *J Nucl Med* 1992;33:339–344.
11. Herholz K, Patlak CS. The influence of tissue heterogeneity on results of fitting nonlinear model equations to regional tracer uptake curves: with an application to compartmental models used in positron emission tomography. *J Cereb Blood Flow Metab* 1987;7:214–229.
12. Kubota R, Yamada S, Kubota K, Ishiwata K, Tamahashi N, Ido T. Intratumoral distribution of fluorine-18-fluorodeoxyglucose in vivo: high accumulation in macrophages and granulation tissues studied by microautoradiography. *J Nucl Med* 1992;33:1972–1980.
13. Hoffman FJ, Huang SC, Phelps ME. Quantitation in positron emission computed tomography: I. Effect of object size. *J Comput Assist Tomogr* 1979;3:299–308.
14. Zasadny KR, Wahl RL. Fit-constrained ("tumor-tailored") parametric images of cancer using FDG [Abstract]. *J Nucl Med* 1993;34:41P.
15. Choi Y, Hawkins RA, Huang SC, et al. Parametric images of myocardial metabolic rate of glucose generated from dynamic cardiac PET 2-[^{18}F]fluoro-2-deoxy-D-glucose studies. *J Nucl Med* 1991;32:733–738.
16. Kim CK, Gupta N, Chandramouli B, Alavi A. Standardized uptake values of FDG corrected for the body surface area are less dependent on the body size than SUVs corrected for the body weight [Abstract]. *J Nucl Med* 1993;34:73P.
17. Gupta NC, Chandramouli B, Frank A, Dewan N, Scott W. PET-FDG imaging for estimating probability of malignancy in solitary pulmonary nodules [Abstract]. *Radiology* 1993;147(suppl):189P.
18. Hamberg LM, Hunter GJ, Alpert NM, Choi NC, Babich JW, Fischman AJ. The dose uptake ratio as an index of glucose metabolism: useful parameter or oversimplification? *J Nucl Med* 1994;35:1308–1312.

Noninvasive Quantification of Dopamine D2 Receptors with Iodine-123-IBF SPECT

Masanori Ichise, James R. Ballinger, Haim Golan, Douglass Vines, Angela Luong, Scott Tsai and Hank F. Kung

Department of Nuclear Medicine, Mount Sinai Hospital, Department of Nuclear Medicine, Princess Margaret Hospital, University of Toronto, Toronto, Ontario Canada; and Division of Nuclear Medicine and Department of Radiology, University of Pennsylvania, Philadelphia, Pennsylvania

Iodine-123-iodobenzofuran (IBF) is a potent dopamine D2 receptor ligand suited for quantitative receptor studies. The purpose of this study was to evaluate three noninvasive methods of estimating the receptor parameter k_3/k_4 in humans with IBF-SPECT. **Methods:** Scans were acquired every 5 min for 180 min using a triple-headed SPECT system following a bolus injection of IBF (296 ± 37 MBq) in 14 normal volunteers. k_3/k_4 was estimated by the peak equilibrium ratio (R_{PE}) method and two proposed methods: a variation of the graphic method that derives the ratio of ligand distribution volumes (R_V) and area ratio (R_A) method, in which the ratio is calculated from the areas under the specific binding and nondisplaceable activity curves. **Results:** The mean R_{PE}, R_V and R_A were 2.74 ± 0.40, 3.06 ± 0.42 and 2.26 ± 0.28, respectively. Both R_{PE} and R_A underestimated R_V. The relationship between R_{PE} or R_A and R_V was linear ($p \leq 10^{-5}$. R_A showed higher correlation ($r = 0.94$) with R_V than did R_{PE} ($r = 0.90$). Simulations based on a tracer kinetic model showed that R_V, unlike R_{PE} or R_A, is affected by neither regional cerebral blood flow (rCBF) nor peripheral clearance rate (CR) of IBF. All three measures showed a significant decline with increasing age ($r = 0.54–0.58$, $p < 0.05$). **Conclusion:** R_V is preferred because it provides a theoretically valid estimate of k_3/k_4, independently of rCBF or CR. Alternatively, R_A might be preferred to R_{PE} because the former is simpler than the latter to implement yet the former provides a measure that equally well correlates with k_3/k_4.

Key Words: iodine-123-IBF; dopamine D2 receptors; brain SPECT; noninvasive quantification

J Nucl Med 1996; 37:513–520

The clinical usefulness of dopamine D2 receptor imaging using SPECT and [^{123}I]iodobenzamide (IBZM) (*1*) has been recently evaluated in several neuropsychiatric conditions (*2–9*). The more recently introduced [^{123}I]iodobenzofuran (IBF) (*10*) binds reversibly to D2 receptors with significantly higher affinity (K_D = 0.11 n*M*) and slightly lower lipophilicity compared with IBZM (*11*), provides higher image contrast and is suited for quantitative receptor studies (*12–14*).

For SPECT imaging of D2 receptors to be widely used, readily accessible yet valid methods to obtain quantitative information about the receptor are needed. In their recent IBF-SPECT study, Laruelle et al. (*14*) were able to measure the binding potential ($BP = B_{max}/K_D$) by using either kinetic or graphic analysis models. These methods, however, are not only invasive, requiring repeated arterial blood sampling, but also are technically demanding, requiring accurate measurements of both tissue and metabolite-corrected plasma concentrations as well as accurate cross-calibrations between the two types of measurements. Furthermore, there were marked individual differences in the rate of both peripheral metabolism and clearance of IBF with unmetabolized, free IBF representing only a small fraction in arterial plasma, and errors in the measurement of this fraction might have a significant effect on the binding potential estimation. Hence, they proposed alternatively to measure the receptor parameter k_3/k_4, the ratio of the transfer constants between the intracerebral nondisplaceable and specifically bound receptor compartments because this measure is independent of the free fraction of IBF.

On the other hand, the traditionally used empirical ratio method does not require blood sampling. Its outcome measure is obtained by calculating a basal ganglia-to-frontal cortex or

Received Jan. 12, 1995; revision accepted Jul. 5, 1995.

For correspondence or reprints contact: Masanori Ichise, MD, FRCP(C), Room 635, Nuclear Medicine, Department of Medical Imaging, Mount Sinai Hospital, 600 University Ave., Toronto, Ontario, Canada M5G 1X5.

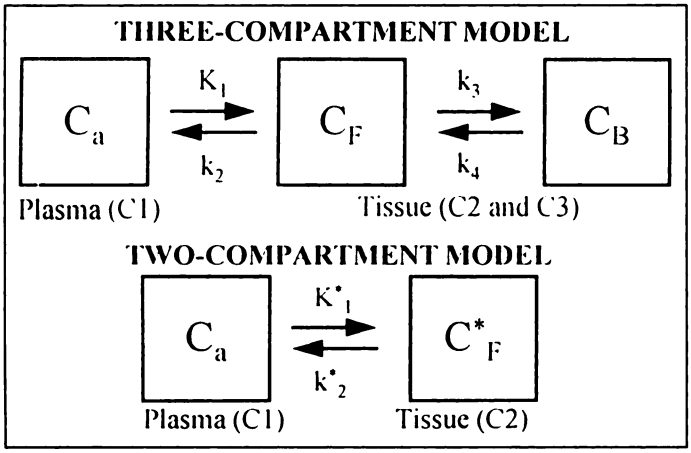

FIGURE 1. Three- and two-compartment models used to describe IBF kinetics. C_a = arterial plasma concentration; C_F, C_F^* = free tissue concentration in the basal ganglia and the frontal cortex, respectively; C_B = specifically bound tissue concentration in the basal ganglia.

cerebellum ratio at a fixed time after a bolus injection of ligand. Laruelle et al. (*14*), however, showed that this measure can be significantly affected by intersubject differences in the peripheral clearance rate (CR) of IBF. Nevertheless, this ratio should provide an estimation of k_3/k_4 if it is obtained according to the peak equilibrium ratio (R_{PE}) method of Farde et al. (*15*).

The purpose of the present study is to evaluate three noninvasive methods to estimate the D2 receptor parameter k_3/k_4 in humans with IBF-SPECT: the R_{PE} method and two proposed methods, including a variation of the graphic method (*16*) that derives the ratio of ligand distribution volumes (R_V) and the area ratio (R_A) method in which the ratio is calculated from the areas under the specific binding and nondisplaceable activity curves based on the steady-state principle of reversible ligand binding (*17*).

THEORY

Peak Equilibrium Ratio Method

Equilibrium analysis of reversible radioligand binding (*15*) represents a special case of multicompartmental kinetic analysis (*18*). The compartment models (Fig. 1) include plasma (C1), nondisplaceable (C2) and receptor (C3) compartments for the receptor-rich basal ganglia, whereas only C1 and C2 are included in the receptor-devoid frontal cortex. Although C2 includes free and nonspecifically bound subcompartments, the nonspecific binding is assumed to be in equilibrium at all times and its magnitude [<5% with IBF (*10*)] is considered negligible. The ligand behavior in these compartments is characterized by the kinetic parameters: K_1 and K_1^* are delivery rate constants in the basal ganglia and the frontal cortex, respectively, and equal the product of blood flow (rCBF) and extraction fraction whereas k_2, k_2^*, k_3 and k_4 are first order rate constants (Fig. 1). If we define the equilibrium distribution volume (EDV), V_i, as the concentration ratio of the ith tissue compartment to free ligand in plasma at equilibrium, IBF activity in the basal ganglia ($C_{BG}(t)$) and the frontal cortex ($C_{FC}(t)$) at equilibrium can be expressed, respectively, as:

$$C_{BG}(t_e) = [V_2 + V_3 + V_P]fC_a(t_e), \quad \text{Eq. 1}$$

$$C_{FC}(t_e) = [V_2^* + V_P]fC_a(t_e), \quad \text{Eq. 2}$$

where f represents the free fraction of total metabolite-corrected plasma IBF concentrations, t_e is time at which equilibrium is established and V_P and $C_a(t)$ are plasma volumes within the tissue and the total plasma concentration, respectively. If we neglect V_P, which represents a small fraction of the total EDV (*19*), then the ratio of the specific (basal ganglia minus frontal cortex) to nondisplaceable (frontal cortex) IBF activity at equilibrium (equilibrium ratio, R_E) can be expressed as:

$$R_E = \frac{C_{BG}(t_e) - C_{FC}(t_e)}{C_{FC}(t_e)} = \frac{[(V_3 + V_2) - V_2^*]fC_a(t_e)}{V_2^*fC_a(t_e)} = \frac{V_3}{V_2}, \quad \text{Eq. 3}$$

provided that $V_2 = V_2^*$. The binding potential or B_{max}/K_D is identical to V_3 (*14*) in experiments using tracer doses of radioligand and $V_3/V_2 = k_3/k_4$ (Appendix A): hence,

$$R_E = \frac{V_3}{V_2} = \frac{BP}{V_2} = \frac{k_3}{k_4}. \quad \text{Eq. 4}$$

In the R_{PE} method (*15*), the ratio (R_{PE}) is calculated when specific binding reaches a peak. R_{PE} is identical to R_E if equilibrium is established at this peak time in all compartments simultaneously. However, this condition may not be met using a single bolus injection technique (*20*).

Variation of Graphic Method

The regional time course of IBF activity after a bolus injection can be analyzed graphically according to the equations (*16*),

$$\frac{\int_0^t C_{BG}(t)dt}{C_{BG}(t)} = a\frac{\int_0^t fC_a(t)dt}{C_{BG}(t)} + b, \quad \text{Eq. 5}$$

$$\frac{\int_0^t C_{FC}(t)dt}{C_{FC}(t)} = a'\frac{\int_0^t fC_a(t)dt}{C_{FC}(t)} + b', \quad \text{Eq. 6}$$

for times in which the transport of ligand from plasma to tissue is unidirectional, where a, a′, b and b′ are constants. Now, combine Equations 5 and 6 by eliminating $\int_0^t fC_a(t)dt$ to yield (Appendix B):

$$\frac{\int_0^t C_{BG}(t)dt}{C_{BG}(t)} = \left(\frac{a}{a'}\right)\frac{\int_0^t C_{FC}(t)dt}{C_{BG}(t)} + \left(-\frac{ab'}{a'}\right)\frac{C_{FC}(t)}{C_{BG}(t)} + b. \quad \text{Eq. 7}$$

Equation 7 is a multilinear equation with partial regression coefficients, a/a′, −ab′/a′ and b. Although this linear relationship cannot be graphically analyzed using conventional graph plotting techniques, these coefficients can be obtained by multiple regression analysis. The coefficient a/a′ is related to EDV as follows (*16*):

$$\frac{a}{a'} = \frac{V_2 + V_3 + V_P}{V_2^* + V_P}. \quad \text{Eq. 8}$$

If we neglect V_P, then the ratio of V_3 to V_2 (R_V),

$$R_V = \frac{V_3}{V_2} = \frac{k_3}{k_4} = \frac{a - a'}{a'} = \frac{a}{a'} - 1, \quad \text{Eq. 9}$$

provided that $V_2 = V_2^*$ or $K_1/k_2 = K_1^*/k_2^*$ (Appendix A).

Area Ratio Method

According to the steady-state principle applicable to reversibly binding ligands, the regional EDV of the ligand, V, also can be calculated by the following equation (*17*):

$$V = \frac{\int_0^\infty C_{RB}(t)dt}{\int_0^\infty fC_a(t)dt}, \qquad \text{Eq. 10}$$

where $C_{RB}(t)$ represents regional brain activity. We can set up two equations, one for the basal ganglia and the other for the frontal cortex, which can be combined to yield one equation excluding $fC_a(t)$ in the same manner as shown in the previous section. Then, the ratio of the areas (R_A) under the specific binding and nondisplaceable activity curves can be expressed as:

$$R_A = \frac{\int_0^t C_{BG}(t)dt - \int_0^t C_{FC}(t)dt}{\int_0^t C_{FC}(t)dt} \rightarrow \frac{(V_3 + V_2) - V_2^*}{V_2^*}$$

$$= \frac{V_3}{V_2} = \frac{k_3}{k_4} \text{ as } t \rightarrow \infty, \qquad \text{Eq. 11}$$

provided that $K_1/k_2 = K_1^*/k_2^*$.

METHODS

Subjects

The subjects consisted of 14 healthy volunteers (7 women, 7 men, mean age 31.5 ± 10 yr) with no current or past history of neuropsychiatric disorders or family history of movement disorders based on a screening interview. All subjects were free of any drugs. Prior to and after the IBF study, subjects were given 400 mg of potassium perchlorate orally. They all gave written informed consent. The study was approved by the Human Subjects Review Committee of the University of Toronto.

Iodine-123-IBF Labeling

Labeling of [^{123}I]IBF was performed by the iododestannylation method developed by Murphy et al. (*21*) adapted to a kit procedure (*22*). Following the labeling reaction with 370–925 MBq (10–25 mCi) sodium [^{123}I]iodide in 0.1 N NaOH, the product was eluted from a C-18 solid-phase extraction cartridge (Sep-Pak Classic, Waters Associates, Milford, MA) with 1 ml absolute ethanol, diluted with 9 ml saline and 100 μl ascorbic acid (1 mg/ml), and sterilized by passage through a 0.22-μm membrane filter. The radiochemical purity was checked by chromatography on ITLC-SG strips developed with chloroform-methanol (9:1). In nine preparations, the radiochemical yield was 85% ± 7% and the radiochemical purity was 96% ± 3%. Retrospective sterility testing was negative.

SPECT

SPECT imaging was performed using a triple-headed system equipped with ultra-high resolution fan-beam collimators and interfaced to a dedicated computer. Prior to imaging, five fiducial markers containing 2 μCi ^{99m}Tc were taped, two on each side of the subject's head at the level of the canthomeatal line (CML) and one on the glabella. Each subject received an intravenous injection of 296 ± 37 MBq (8 ± 1 mCi) IBF over 30 sec with the head securely positioned in a head holder. Scans were acquired every 5 min, starting at the midpoint of injection using continuous scan mode for 180 min. For each scan, one hundred twenty 7.5-sec projection images were obtained using

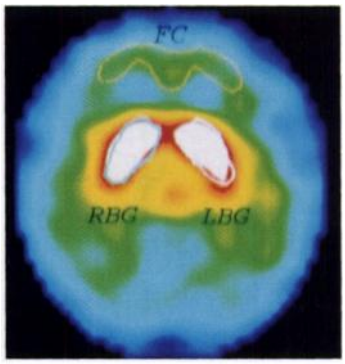

FIGURE 2. Transaxial IBF SPECT image at the level of the striatum parallel to the canthomeatal line with superimposed ROIs. RBG = right basal ganglia; LBG = left basal ganglia; FC = frontal cortex.

3° angle intervals on a 128 × 128 matrix over 360° by rotating each detector head 120°. The radius of rotation was fixed at 13.5 cm. Using a Jaszczak phantom (model 7000, Data Spectrum Corp.) and capillary ^{123}I line sources, the FWHM was 9.1 mm in water at the center of the field of view. To monitor system sensitivity, each of five plastic cylindrical phantoms (60 cm^2 × 20 cm = 1200 ml) filled with a uniform solution of varying activities [18.5–55.5 MBq (0.5–1.5 mCi)] of ^{123}I was scanned on the day of experiment. The mean sensitivity of the system was 612 ± 12 cpm/μCi and varied less than 2% and 5% within and between the experiments, respectively. Deadtime count losses over this activity range were negligible.

Prior to tomographic reconstruction, raw data from two consecutive 5-min scans were added to create 18 sets of 10-min scans, and each dataset was folded onto a 64 × 64 matrix. One-pixel thick (4.33 mm) transaxial slices from the vertex of the brain to the level of the CML were reconstructed parallel to the CML using a three-dimensional Butterworth postfilter (order = 10, cutoff frequency = 0.25) after applying a ramp backprojection filter. Attenuation correction was performed by assuming uniform attenuation equal to that of water (μ = 0.15 cm^{-1}) (*23*) within an ellipse drawn around the skull as identified by the fiducial markers.

Data Analysis

From each set of transaxial images, four consecutive slices (1.73 cm thick) corresponding to the highest signal in the basal ganglia were summed. Regions of interest (ROIs) were placed using templates over the right and left basal ganglia (volume = 4.87 cm^3 each) and frontal cortex (volume = 6.82 cm^3) (Fig. 2). The basal ganglia templates were created by outlining the transaxial section of the basal ganglia in the Talairach's stereotaxic brain atlas (*24*) with the area of template fixed at 2.81 cm^2. The frontal cortex template was created individually by drawing an irregular ROI (area = 3.93 cm^2) over the frontal cortex on the summed image of the first dataset (representing rCBF image). ROI placement depended on visual identification of anatomical regions aided by the stereotaxic atlas. All ROIs were applied by the same investigator (M.I.) to eliminate interobserver variation. Average counts per pixel from each region were decay-corrected for the time of injection. Counts from the right and left basal ganglia were averaged. No attempts were made to correct for partial volume or scatter effects.

R_{PE} was obtained according to the method of Farde et al. (*15,25,26*): a Levenberg-Marquardt least squares minimization technique (*27*) was used for curve fitting, implemented in GRAPHPAD PRIZM (Graphpad Software, Inc., San Diego, CA). The a/a′ was derived by multilinear regression analysis. The integrals in Equation 7 were obtained numerically using the trapezoid rule. All data points were included in the analysis based on the posthoc runs with varying the number of data points in which a/a′ had the largest t statistic and the smallest

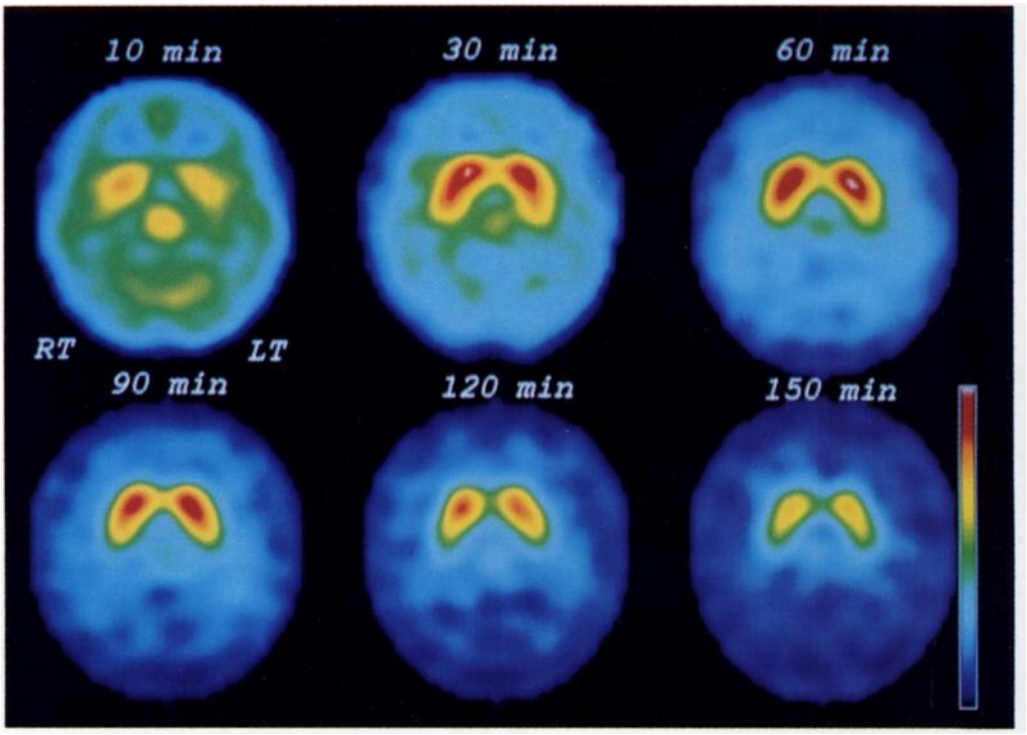

FIGURE 3. Serial transaxial IBF-SPECT images (10–150 min postinjection) at the level of the striatum in a 19-yr-old woman (study no. 1). Basal ganglia IBF uptake in this subject peaked at 48 min just prior to the 60-min image followed by a specific binding peak during the 90-min scan.

standard error of estimate [expressed as percent coefficient of variation (CV)] when all data points were included. R_V was obtained by subtracting 1 from a/a′. R_A was calculated using all the 3-hr data. To determine the minimum duration of scanning needed to derive meaningful values of R_V and R_A, these measures were calculated using data corresponding to increasing lengths of experiment from 60 to 180 min postinjection in 10-min increments. Two-tailed Student's t-test for paired samples were used to compare outcome-measure groups. The relationships between three outcome measures were analyzed by calculating Pearson correlation coefficients. Simple linear regression analysis was used to test for significant effects of age on three outcome measures. Statistical significance was defined as $p < 0.05$. Summaries of study variables were expressed as mean ± s.d..

Simulations

To investigate the potential effect of rCBF and CR on three outcome measures, brain response curves were simulated by analytical solutions of Equations 12–14 (*18*) using hypothetical sets of kinetic parameters and arterial input functions selected from those reported previously (*14*). For the basal ganglia, the following parameters were used: $K_1 = 0.12$ ml g^{-1} min^{-1}, $k_2 = 0.048$ min^{-1}, $k_3 = 0.90$ min^{-1}, $k_4 = 0.036$ min^{-1} ($K_1/k_2 = 2.50$, $k_3/k_4 = 2.50$). For the frontal cortex, seven sets of K_1^* were used, including 0.12, 0.11, 0.10, 0.09, 0.08, 0.07 and 0.06 ml g^{-1} min^{-1} with K_1^*/k_2^* constrained at 2.50. The arterial input functions were given as a sum of three exponentials with the first two time constants, $\lambda_1 = 1.69$ min^{-1}, $\lambda_2 = 0.082$ min^{-1} and three sets of the terminal time constant, $\lambda_3 = 0.0071$ (average clearance), 0.0135 (fast clearance) and 0.0028 min^{-1} (slow clearance). For each set of parameters, R_{PE}, R_V and R_A were calculated using the data created for the initial 180 min, respectively. Simulations were implemented in MATHCAD (Math Soft, Inc., Cambridge, MA).

RESULTS

Basal ganglia activities showed a peak uptake at 55 ± 16 min (range 33–88 min) postinjection and slower washout than that for the frontal cortex, whereas the frontal cortex activities showed an early peak uptake (<20 min) and rapid washout. Specific binding activities showed a peak occurring later (91 ± 15 min, range 67–114 min) than that for the basal ganglia. Selected IBF images of a 19-yr-old woman (study no. 1) are shown in Figure 3, and the corresponding regional IBF time-activity curves in Figure 4.

The a/a′ (4.06 ± 0.42) had highest t values (63 ± 19, $p < 10^{-5}$) and smallest CVs of 1.8% ± 0.6% with highly significant overall regression (F = 5000 ± 2000, r = 0.9991 ± 0.0005, $p < 10^{-6}$) when all 18 data points were included. The mean R_V was 3.06 ± 0.42. All specific binding peaks were identified as a point in time by setting the derivative of the fitted curve to zero. The mean R_{PE} was 2.74 ± 0.40, which was lower than that of R_V ($p < 10^{-4}$). The mean R_A was 2.26 ± 0.28 which was lower than that of R_{PE} ($p < 10^{-4}$). Table 1 summarizes the individual values of the three outcome measures. The relationship between R_{PE} or R_A and R_V was linear with slopes of 0.87 and 0.63, respectively (Fig. 5). R_A showed a higher correlation

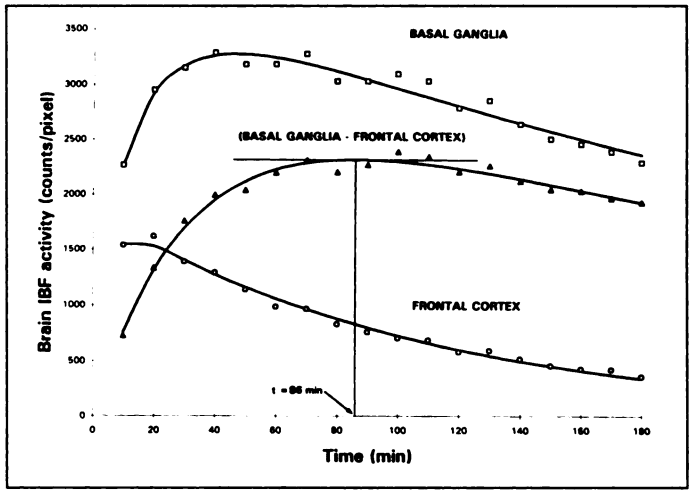

FIGURE 4. Regional IBF activity curves of a 19-yr-old woman (study no. 1). $C_{BG}(t)$ (indicated by □), $C_{FC}(t)$ (indicated by ○) and $C_{BG}(t)$-$C_{FC}(t)$ (indicated by Δ) were fitted to a sum of three exponentials (solid lines), respectively. The vertical line indicates the peak time when the derivative of the specific binding curve is zero (horizontal line).

TABLE 1
Measurement of Dopamine D2 Receptor Parameter k_3/k_4 with IBF-SPECT by Peak Equilibrium (R_{PE}), Variation of Graphic (R_V) and Area Ratio (R_A) Methods

Subject no.	Age (yr)	Sex	R_{PE}	R_V	R_A
1	19	F	2.79	3.31	2.37
2	22	F	3.13	3.66	2.64
3	23	F	2.54	3.01	2.31
4	25	F	2.86	2.99	2.26
5	25	F	2.76	2.85	2.09
6	33	F	2.80	3.04	2.10
7	38	F	2.56	2.76	1.99
8	22	M	2.79	2.95	2.27
9	23	M	3.62	3.78	2.76
10	34	M	2.82	3.41	2.65
11	41	M	2.05	2.61	1.89
12	44	M	2.90	3.24	2.33
13	46	M	2.77	3.01	2.10
14	47	M	1.98	2.16	1.84
Mean ± s.d.	31.5 ± 10		2.74 ± 0.40	3.06 ± 0.42	2.26 ± 0.28

($r = 0.94$, $p = 10^{-6}$) with R_V than did R_{PE} ($r = 0.90$, $p = 10^{-5}$), although R_A was more markedly underestimated R_V than did R_{PE}. All three measures declined significantly with increasing age at 6.5% per decade ($r = 0.54-0.58$, $p < 0.05$).

Scanning Duration and R_V or R_A

For $60 \leq t < 90$ min, the regression for a/a′ was significant in most cases, with $p < 10^{-3}$. The a/a′, however, was underestimated at 82% of the value measured at 180 min with CV of 12%. For $90 \leq t \leq 180$ min, the regression for a/a′ was significant with $p < 10^{-5}$ in all cases with a/a′ increasingly approaching to the final value and smaller CV as the scanning time is increased. At 120 min, R_V was 94% ± 5% of the value at 180 min. For $60 \leq t \leq 180$ min, R_A was always linear with R_V ($p = 10^{-6} - 2 \times 10^{-3}$). R_A progressively underestimated R_V with the smaller r values as the scanning time was decreased. The mean R_A values were 1.83 ± 0.24 and 1.21 ± 0.18 at 120 and 60 min, respectively. R_A showed a higher correlation with R_V for $140 \leq t \leq 180$ min, than did R_{PE} with R_V (at 140 min, $R_A = 1.99 \pm 0.25$, slope = 0.55, r = 0.91, and $p = 10^{-6}$).

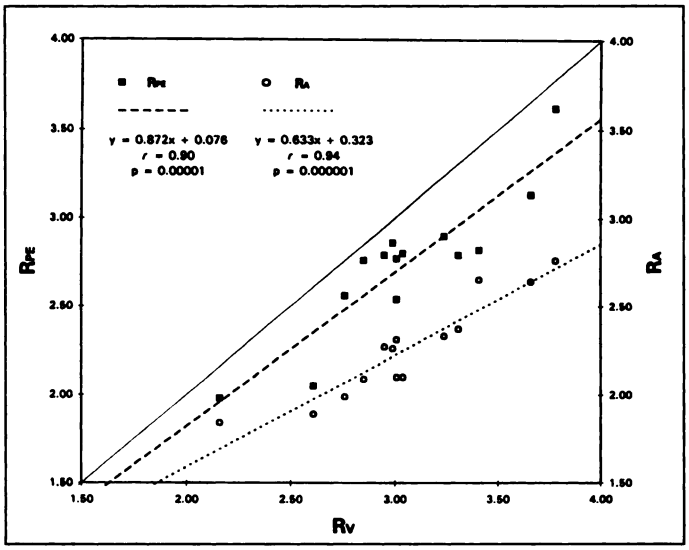

FIGURE 5. Relationship between R_{PE} (indicated by ■) or R_A (indicated by ○) and R_V. The solid line represents the line of identity with R_V. The coarse and fine dotted lines represent linear regressions of R_{PE} and R_A, respectively. For a detailed description, refer to the text.

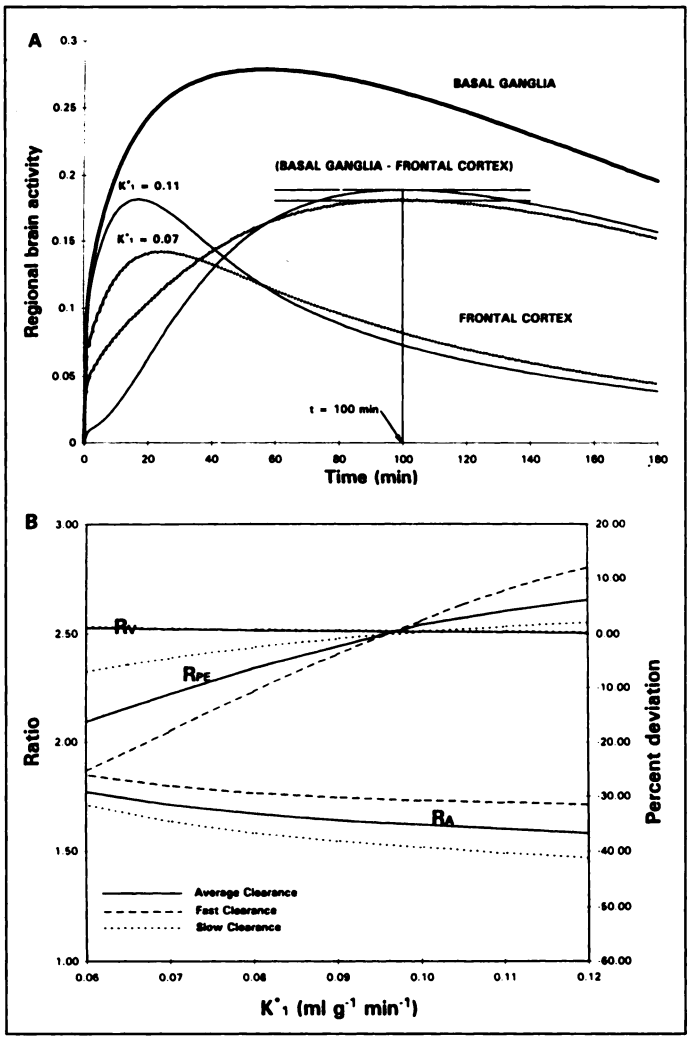

FIGURE 6. (A) Simulated regional brain time-activity curves show the effect of rCBF on R_{PE}. Two sets of curves represent high rCBF ($K_1^* = 0.11$ ml g^{-1} min^{-1}, thin solid curves) and low rCBF ($K_1^* = 0.07$ ml g^{-1} min^{-1}, dotted curves). For a detailed description, refer to the text. (B) Effect of rCBF and the peripheral clearance rate (CR) on R_V, R_{PE} and R_A. K_1^* was varied along the x-axis. The primary y-axis (left) indicates the magnitude of R_V, R_{PE} or R_A, while the secondary y-axis (right) indicates the percent deviation of these measures from the value of $k_3/k_4 = 2.50$. Each outcome measure is plotted for three sets of CR: average (solid curve), fast (coarse dotted curve) and slow (fine dotted curve) CRs. R_V was derived from the 16 timepoint data with 10-min intervals from 20 to 180 min. For a detailed description, refer to the text.

Simulations

Figure 6A illustrates the effect of rCBF on R_{PE}. With CR kept constant at the average rate, two sets of simulated frontal and specific binding activity curves are shown, corresponding to $K_1^* = 0.11$ (thin solid curves) and 0.07 ml · g^1 · min^1 (dotted curves), respectively. Although the specific binding peak times for both curves are seen at approximately the same time (t = 100 min), R_{PE} in the former instance (2.60) overestimates, and in the latter instance (2.22) underestimates k_3/k_4 (2.50). Figure 6B shows plots of R_V, R_{PE} and R_A as K_1^* is varied from 0.06 to 0.12 ml g^{-1} min^1 and as CR is varied. R_V (2.51 ± 0.01) is affected little by changes in rCBF or CR whereas both R_{PE} (2.41 ± 0.23) and R_A (1.66 ± 0.10) can be significantly affected not only by rCBF but also by CR. R_{PE} is close to the value of k_3/k_4 with negligible effects of CR when K_1^* is 0.10 ml g^{-1} min^{-1}. Otherwise, R_{PE} either progressively underestimates or overestimates k_3/k_4 as K_1^* decreases or increases from this point with progressively more marked effects of CR. On the

other hand, R_A consistently underestimates k_3/k_4 at relatively constant levels over a wide range of K_1^* with relatively constant effects of CR (Fig. 6B).

DISCUSSION

In this study, we compared the results of three noninvasive methods to measure the D2 receptor parameter k_3/k_4 in humans with IBF SPECT. Each method is theoretically supported to provide estimates of k_3/k_4. Certain assumptions must be met, including the one common to all, whereby V_2 is identical in both the basal ganglia and frontal cortex. This assumption is widely employed in receptor quantification studies with PET because it can improve identifiability and physiological meaning of the rate constants (*18,26*). k_3/k_4 should reflect the binding potential, provided that V_2 is uniform across subjects. This latter assumption appears reasonable because V_2 showed the lowest between-subject variation of all the outcome measures reported previously (*14*). We made no direct comparison in our study of the three outcome measures to the results of kinetic modeling studies with arterial input functions. To compensate for this limitation, however, we performed simulation experiments in which three outcome measures obtained from the hypothetical datasets were compared to the value of k_3/k_4 set by the standard kinetic model and the effects of rCBF and CR upon these measures were evaluated.

The R_V method presented in this study shows that determination of the ratio of EDVs does not require the knowledge of arterial plasma ligand concentrations. R_V should be theoretically the same as that obtained by the original graphic method with arterial input functions. Unlike R_{PE} or R_A, R_V is not affected by rCBF or CR. This technique, then, might allow selection of reference regions with low rCBF such as the white matter. This might be an important consideration for other types of receptor studies, such as those of benzodiazepine receptors present in all cortical regions except the white matter (*28*). The mean value of R_V (3.06 ± 0.42) in our study was slightly higher than that (2.48 ± 0.83) reported by Laurelle et al. (*14*). Both subject populations were similar in age (31.5 ± 10 yr versus 28 ± 7 yr). Our higher value might be partly related to our use of considerably smaller basal ganglia ROIs (4.87 cm^3) than theirs (11.25 cm^3), which likely resulted in a smaller contribution of the low rCBF white matter to our basal ganglia ROI due to the partial volume effect. Billings et al. (*29*), however, showed that the target-to-background IBF ratio measured by SPECT (3.5) significantly underestimated the ratio (17.8) determined by ex vivo autoradiography. This is presumably due to multiple factors, including partial volume effects, attenuation, scattering, filtering and statistical limitations which all contribute to errors in the estimation of real radioactivity in the ROI. It therefore appears important to make measurements under identical imaging conditions to ensure a meaningful comparison of receptor parameter values between subjects.

The empirical ratio can be significantly affected by rCBF or CR (*14*). R_{PE}, however, is not entirely independent of rCBF or CR either, although the latter should be affected by these factors to a lesser degree than the former. This effect of rCBF or CR on R_{PE} provides indirect evidence that equilibrium may never be reached simultaneously in all compartments when specific binding reaches a peak with a bolus injection technique (*20*). R_{PE} (2.74 ± 0.40) in this study underestimated R_V (3.06 ± 0.42), which presumably reflects a larger contribution of the low rCBF white matter in our frontal cortex ROI compared with that in the basal ganglia ROI. Our simulation data suggest that the effect of both rCBF and CR on R_{PE} are progressively more marked as rCBF in the reference region decreases.

Simultaneous establishment of equilibrium in all compartments can be achieved by administering a tracer as a combination of bolus and constant infusion (*20,30*). During this prolonged equilibrium, single scan measurements might be feasible (*20*). Although this approach for IBF appears promising (*31*), our simulations (data not shown) suggest that it takes IBF several hours to reach equilibrium and the practicality of this approach must be evaluated. Furthermore, a significant fraction of activity in arterial plasma is a lipophilic metabolite that might cross the blood-brain barrier (*13,14*). Although this effect appears negligible after a bolus injection of IBF (*13*), the significance of prolonged exposure in the constant infusion paradigm needs to be evaluated.

R_A in our study significantly underestimated both R_V and R_{PE}. This is because R_A was calculated from the data obtained for a finite period of time postinjection during which IBF washout in the frontal cortex is faster than that of the specific binding compartment. R_A, however, showed a higher correlation with R_V than did R_{PE}. This may be partly due to the relatively greater effect of CR on R_{PE} than CR on R_A when K_1^* is significantly smaller than K_1. Considering the effect of low rCBF on R_{PE}, selection and placement of cortical ROIs appear critical for R_{PE}. The task of defining cortical ROIs exclusive of the low rCBF white matter, however, is limited by the inherent spatial resolution of the SPECT system. The R_A method is simpler than the R_{PE} method because the former does not require the analysis of multiple scans to identify the peak specific binding time. A total acquisition time of at least 2 hr is required for R_A to be of a similar level of statistical significance to that of R_{PE} in reflecting k_3/k_4.

We selected the frontal cortex as opposed to the cerebellum or occipital cortex as the reference region for the following reasons:

1. The cerebellum is difficult to localize properly without coregistration with morphological imaging.
2. Previous studies of postmortem human brains with ^{3}H-raclopride (*32*) and ^{125}I-epidepride (*33*) or of in vivo human brain with ^{11}C-raclopride (*25*), as well nonhuman primates with IBF (*29*), have demonstrated that D2 receptor concentrations in the frontal cortex are either not detected or are negligible. Extrastriatal D3 and D4 receptors, however, are found in the limbic frontal lobe with D3 being in the olfactory tubercle (*34,35*). Our in vitro study in collaboration with P. Seeman showed that the affinity of IBF for D4 receptors is negligible (inhibition constant, K_i = 320 n*M*, *unpublished data*). Although IBF is also a potent D3 receptor ligand (K_i = 0.05 n*M*), the orbitofrontal region was not included in our frontal slice.
3. An alternative region would be the occipital cortex, but we felt that the occipital cortex might be more variable in terms of rCBF, depending on the visual stimulation status, than the frontal cortex.

We observed age-dependent variations of the D2 receptor parameter in our subjects, with a 6.5% per decade decline in the age range of 19 to 47 yr. This decline is larger than that found previously with IBZM-SPECT (1.5% per decade) (*3*) but consistent with those found with ^{11}C-raclopride PET [6% per decade (*36*) and 4.6% per decade (*37*)]. On the other hand, a postmortem study showed a 2.2% per decade decline (*38*). More data, including subjects with wider age ranges, are required for complete elucidation of this finding with IBF.

CONCLUSION

Three noninvasive methods to obtain quantitative information about the D2 receptor with IBF-SPECT were evaluated. The R_V method is preferred because it provides a theoretically valid estimate of the receptor parameter k_3/k_4 independently of rCBF or CR. Alternatively, the R_A method might be preferred to the R_{PE} method because the former is simpler than the latter to implement, yet the former provides a measure that correlates equally well with k_3/k_4. The limitation of these methods is that multiple SPECT scans with a total acquisition time of at least 2 hr are required. Further refinements to improve on "practicality" as well as repeated studies to address the issue of the reproducibility of these methods are needed.

APPENDIX A

Three- and two-compartment models are described by the following set of differential equations:

$$\frac{dC_F(t)}{dt} = K_1 f C_a(t) - k_2 C_F(t) - k_3 C_F(t) + k_4 C_B(t), \quad \text{Eq. 12}$$

$$\frac{dC_B(t)}{dt} = k_3 C_F(t) - k_4 C_B(t), \quad \text{Eq. 13}$$

$$\frac{dC_F^*(t)}{dt} = K_1^* f C_a(t) - k_2^* C_F^*(t). \quad \text{Eq. 14}$$

By simply setting all derivatives (Eqs. 12–13) to zero, we obtain V_i in terms of kinetic parameters as follows:

$$V_2 = \frac{K_1}{fk_2} \text{ and } V_2^* = \frac{K_1^*}{fk_2^*}, \quad \text{Eq. 15}$$

$$V_3 = \frac{K_1 k_3}{fk_2 k_4}, \quad \text{Eq. 16}$$

$$\therefore \frac{V_3}{V_2} = \frac{k_3}{k_4}. \quad \text{Eq. 17}$$

For symbol definitions, refer to the text.

APPENDIX B

Equation 7 is obtained as follows: First, rearrange Equation 6,

$$\int_0^t f C_a(t)dt = \frac{C_{FC}(t)}{a'}\left(\frac{\int_0^t C_{FC}(t)dt}{C_{FC}(t)} - b'\right). \quad \text{Eq. 18}$$

Insert Equation 18 into Equation 5,

$$\frac{\int_0^t C_{BG}(t)dt}{C_{BG}(t)} = \left(\frac{a}{a'}\right)\frac{C_{FR}(t)\left(\frac{\int_0^t C_{FC}(t)dt}{C_{BG}(t)} - b'\right)}{C_{BG}(t)} + b. \quad \text{Eq. 19}$$

Rearrange Equation 19 to yield Equation 7.

ACKNOWLEDGMENTS

The authors thank Bruce Gray, MD, Hiroshi Toyama, MD, Kaname Matsumura, MD and Hiromichi Nakashima, MD for valuable suggestions. This work was supported by the SPECT Research Fund from the Department of Medical Imaging, Mount Sinai Hospital and partly supported by Picker International Canada Inc.

REFERENCES

1. Kung HF, Pan S, Kung MP, et al. In vitro and in vivo evaluation of [^{123}I]IBZM: a potential CNS D-2 dopamine receptor imaging agent. *J Nucl Med* 1989;30:88–92.
2. Brucke T, Podreka I, Angelberger P, et al. Dopamine D2 receptor imaging with SPECT: studies in different neuropsychiatric disorders. *J Cereb Blood Flow Metab* 1991;11:220–228.
3. Ichise M, Toyama H, Fornazzari L, Ballinger JR, Kirsh JC. Iodine-123-IBZM dopamine D2 receptor and technetium-99m-HMPAO brain perfusion SPECT in the evaluation of patients with and subjects at risk for Huntington's disease. *J Nucl Med* 1993;34:1274–1281.
4. Oertel WH, Schwarz J, Tatsch K, Arnold G, Gasser T, Kirsch CM. IBZM-SPECT as predictor for dopamimetic responsiveness of patients with de novo parkinsonian syndrome. *Adv Neurol* 1993;60:519–524.
5. Tatsch K, Schwarz J, Oertel WH, Kirsch CM. SPECT imaging of dopamine D2 receptors with ^{123}I-IBZM: initial experience in controls and patients with Parkinson's syndrome and Wilson's disease. *Nucl Med Commun* 1991;12:699–707.
6. Schwarz J, Tatsch K, Arnold G, et al. ^{123}I-iodobenzamide-SPECT predicts dopaminergic responsiveness in patients with de novo parkinsonism *Neurology* 1992;42:556–561.
7. Laulumaa V, Kuikka JT, Soininen H, Bergstrom K, Lansimies E, Riekkinen P. Imaging of D2 dopamine receptors of patients with Parkinson's disease using single photon emission computed tomography and iodobenzamide ^{123}I. *Arch Neurol* 1993; 50:509–512.
8. van Royen E, Verhoeff NF, Speelman JD, Wolters EC, Kuiper MA, Janssen AG. Multiple system atrophy and progressive supranuclear palsy. Diminished striatal D2 dopamine receptor activity demonstrated by ^{123}I-IBZM single-photon emission computed tomography. *Arch Neurol* 1993;50:513–516.
9. Pilowsky LS, Costa DC, Ell PJ, Murray RM, Verhoeff NP, Kerwin RW. Clozapine, single photon emission tomography and the D2 dopamine receptor blockade hypothesis of schizophrenia. *Lancet* 1992;340:199–202.
10. Kung MP, Kung HF, Billings J, Yang Y, Murphy RA, Alavi A. The characterization of IBF as a new selective dopamine D2 receptor imaging agent. *J Nucl Med* 1990;31:648–654.
11. Kessler RM, Ansari MS, de Paulis T, et al. High affinity dopamine D2 receptor radioligands. 1. Regional rat brain distribution of iodinated benzamides. *J Nucl Med* 1991;32:1593–1600.
12. Al-Tkriti MS, Baldwin RM, Zea-Ponce Y, et al. Comparison of three high affinity SPECT radiotracers for the dopamine D2 receptor. *Nucl Med Biol* 1994;21:179–188.
13. Baldwin RM, Zea-Ponce Y, Zoghbi SS, et al. Pharmacokinetics of the three radioiodinated dopamine D2 receptor ligands [^{123}I]IBF, [^{123}I]epidepride and [^{123}I]2′-ISP in nonhuman primates. *Nucl Med Biol* 1994;21:969–976.
14. Laruelle M, van Dyck C, Abi-Dargham A, et al. Compartmental modeling of iodine-123-iodobenzofuran binding to dopamine D2 receptors in healthy subjects. *J Nucl Med* 1994;35:743–754.
15. Farde L, Hall H, Ehrin E, Sedvall G. Quantitative analysis of D2 dopamine receptor binding in the living human brain by PET. *Science* 1986;231:258–261.
16. Logan J, Fowler JS, Volkow ND, et al. Graphical analysis of reversible radioligand binding from time-activity measurements applied to [N-^{11}C-methyl]-(−)-cocaine PET studies in human subjects. *J Cereb Blood Flow Metab* 1990;10:740–747.
17. Lassen NA. Neuroreceptor quantitation in vivo by the steady-state principle using constant infusion or bolus injection of radioactive tracers. *J Cereb Blood Flow Metab* 1992;12:709–716.
18. Frost JJ, Douglass KH, Mayberg HS, et al. Multicompartmental analysis of [^{11}C]-carfentanil binding to opiate receptors in humans measured by positron emission tomography. *J Cereb Blood Flow Metab* 1989;9:398–409.
19. Phelps ME, Huang SC, Hoffman EJ, Kuhl DE. Validation of tomographic measurement of cerebral blood volume with C-11-labeled carboxyhemoglobin. *J Nucl Med* 1979;20:328–334.
20. Carson RE, Channing MA, Blasberg RG, et al. Comparison of bolus and infusion methods for receptor quantitation: application to [^{18}F]cyclofoxy and positron emission tomography. *J Cereb Blood Flow Metab* 1993;13:24–42.
21. Murphy RA, Kung HF, Kung MP, Billings J. Synthesis and characterization of iodobenzamide analogues: potential D-2 dopamine receptor imaging agents. *J Med Chem* 1990;33:171–178.
22. Billings JJ, Kung MP, Chumpradit S, Mozley D, Alavi A, Kung HF. Characterization of radioiodinated TISCH: a high-affinity and selective ligand for mapping CNS D1 dopamine receptor. *J Neurochem* 1992;58:227–236.
23. Chang L. A method for attenuation correction in radionuclide computed tomography. *IEEE Trans Nucl Sci* 1978;NS-25:638–643.
24. Talairach J, Tournoux P, Rayport M, eds. *Co-planar stereotaxic atlas of the human brain. Three-dimensional proportional system: an approach to cerebral imaging.* New York: Thieme Inc.; 1988:1–122.
25. Farde L, Pauli S, Hall H, et al. Stereoselective binding of ^{11}C-raclopride in living human brain—a search for extrastriatal central D2-dopamine receptors by PET. *Psychopharmacology* 1988;94:471–478.
26. Farde L, Eriksson L, Blomquist G, Halldin C. Kinetic analysis of central [^{11}C]raclopride binding to D2-dopamine receptors studied by PET—a comparison to the equilibrium analysis. *J Cereb Blood Flow Metab* 1989;9:696–708.
27. Levenberg K. A method for the solution of certain problems in least squares. *Q Appl Math* 1944;2:164–168.
28. Abi-Dargham A, Laruelle M, Seibyl J, et al. SPECT measurement of benzodiazepine receptors in human brain with iodine-123-iomazenil: kinetic and equilibrium paradigms. *J Nucl Med* 1994;35:228–238.
29. Billings JJ, Guo YZ, Kung MP, Kung HF. Localization of IBF as a D2 dopamine receptor imaging agent in nonhuman primates. *Eur J Nucl Med* 1993;20:1146–1153.
30. Kawai R, Carson RE, Dunn B, Newman AH, Rice KC, Blasberg RG. Regional brain measurement of B_{max} and K_D with the opiate antagonist cyclofoxy: equilibrium studies in the conscious rat. *J Cereb Blood Flow Metab* 1991;2:529–544.

31. Laruelle M, Abi-Dargham A, Van Dyck CH, et al. D-amphetamine induced dopamine release reduces the binding potential of [^{123}I]IBF for dopamine D2/D3 receptors in humans [Abstract]. *J Nucl Med* 1994;35:84P.
32. Hall H, Farde L, Sedvall G. Human dopamine receptor subtypes—in vitro binding analysis using ^{3}H-SCH 23390 and ^{3}H-raclopride. *J Neural Transm* 1988;73:7–21.
33. Kessler RM, Whetsell WO, Ansari MS, et al. Identification of extrastriatal dopamine D2 receptors in postmortem human brain with [^{125}I]epidepride. *Brain Res* 1993;609: 237–243.
34. Van Tol HH, Bunzow JR, Guan HC, et al. Cloning of the gene for a human dopamine D4 receptor with high affinity for the antipsychotic clozapine. *Nature* 1991;350:610–614.
35. Sokoloff P, Giros B, Martres MP, Bouthenet ML, Schwartz JC. Molecular cloning and characterization of a novel dopamine receptor (D3) as a target for neuroleptics. *Nature* 1990;347:146–151.
36. Antonini A, Leenders KL, Reist H, Thomann R, Beer HF, Locher J. Effect of age on D2 dopamine receptors in normal human brain measured by positron emission tomography and ^{11}C-raclopride. *Arch Neurol* 1993;50:474–480.
37. Rinne JO, Hietala J, Ruotsalainen U, et al. Decrease in human striatal dopamine D2 receptor density with age: a PET study with [^{11}C]raclopride. *J Cereb Blood Flow Metab* 1993;13:310–314.
38. Seeman P, Bzowej NH, Guan HC, et al. Human brain dopamine receptors in children and aging adults. *Synapse* 1987;1:399–404.